Appl. Magn. Reson. (2007) 32, 527–546
DOI 10.1007/s00723-007-0036-x
Printed in The Netherlands

Applied Magnetic Resonance

Multinuclear MAS NMR Investigation of Sol-Gel and Ball-Milled Nanocrystalline Ga_2O_3

L. A. O'Dell[1], **S. L. P. Savin**[2], **A. V. Chadwick**[2], and **M. E. Smith**[1]

[1] Department of Physics, University of Warwick, Coventry, United Kingdom
[2] School of Physical Sciences, University of Kent, Canterbury, United Kingdom

Received 6 November 2006; revised 4 March 2007

Abstract. ^{71}Ga magic-angle spinning (MAS) nuclear magnetic resonance (NMR) has been used to characterize the structural evolution of nanocrystalline Ga_2O_3 samples prepared by sol-gel and ball-milling techniques. ^{29}Si and ^{27}Al MAS NMR have also been used to characterize silica and alumina Zener pinning phases. ^{71}Ga NMR parameters are reported for the α- and β-Ga_2O_3 phases, and more tentatively for the δ-Ga_2O_3 phase. By simulating the octahedrally coordinated gallium NMR line of β-Ga_2O_3 using Gaussian distributions in χ_Q, the extent of disorder in the Ga_2O_3 crystallites has been quantified. The ball-milled samples contain much more inherent disorder than the sol-gel samples in the nano-phase, which was observed from simulations of the ^{71}Ga MAS NMR spectra. The silica pinning phase produced highly crystalline and densely aggregated nanocrystalline Ga_2O_3, as well as the smallest nanocrystal sizes.

1 Introduction

Ga_2O_3 commonly exists in the stable β-phase, although other phases exist, such as α, γ, δ, and ε, each of which eventually transform to β upon heating [1, 2]. Gallium oxide compounds exhibit close analogies to the Al_2O_3 system [2, 3], with many of the same structures occurring in both systems, for example, β-Ga_2O_3 shares the same structure as θ-Al_2O_3 [4], with gallium atoms distributed equally between tetrahedral and octahedral sites [3]. The α-Ga_2O_3 structure is the same as corundum (α-Al_2O_3), while the structures of the γ-, δ- and ε-Ga_2O_3 phases are not universally agreed upon [5], although γ and ε are thought to be defect spinel structures similar to transition alumina phases [4], and δ is reported to exist in a C-type rare-earth oxide structure [6]. The δ-phase has been observed to transform to ε before finally reaching the β-phase [2]. Gallium and aluminium tend to exist in the same oxidation states and prefer tetrahedral and octahedral coordinations, and can form $GaAlO_3$ [7], although at higher temperatures (about 1200 °C) the α-Al_2O_3 and β-Ga_2O_3 phases tend to separate out [5].

β-Ga_2O_3 is used as a high-temperature oxygen sensor, in the range of 800–1000 °C [8, 9]. Since gas-sensing properties are expected to improve at lower crystallite sizes (due to an increased surface area), stabilizing nanocrystalline β-Ga_2O_3 in this temperature range would be highly advantageous for this application. The material is also used widely in catalysis, with the Ga_2O_3-Al_2O_3 system showing favorable properties [7, 10], and so Zener pinning (as quoted in ref. 11) the nanocrystalline phase with alumina could result in a very useful material.

Gallium has two nuclear magnetic resonance (NMR) active nuclear isotopes, both with nuclear spin $I = 3/2$, ^{69}Ga and ^{71}Ga, with natural abundances of 60.1% and 39.9%, respectively [12]. ^{71}Ga NMR is favored over ^{69}Ga because of its higher Larmor frequency and smaller quadrupole moment, which means that it suffers less second-order quadrupolar broadening [13] (by a factor of 3.25 [3]). As the structures of Ga_2O_3 can be similar to those of Al_2O_3, ^{71}Ga NMR shares similarities with ^{27}Al, with spectral peaks visible due to four-, five- and six-coordinated gallium environments present at chemical shifts that become more negative with increasing coordination [3, 4]. Some NMR parameters for β-Ga_2O_3 have already been reported for a twinned sample [14] and very recently for a powder sample [15]. The biggest disadvantage of ^{71}Ga magic-angle spinning (MAS) NMR over ^{27}Al is the larger second-order quadrupolar broadening (by a factor of about 2), which results in significant overlapping of the different spectral features as well as broad spinning sidebands in the MAS spectra which can make accurate spectral deconvolution very challenging (these do not apply to single-crystal studies). In this investigation, ^{71}Ga MAS NMR has been used to characterize the various phases present in nanocrystalline Ga_2O_3 samples produced by sol-gel and ball-milling methods. In order to stabilize the nanocrystals against excessive grain growth during the annealing stage, silica and alumina Zener pinning phases have been introduced, which have already been shown to limit grain growth in nanocrystalline metal oxides [16–18] and have been previously studied by ^{29}Si and ^{27}Al NMR in nanocrystalline SnO_2 [19], MgO [20] and ZrO_2 [20] systems. These silica and alumina pinning phases are also investigated here.

2 Experimental Details

2.1 Sample Preparation

2.1.1 Sol-Gel Ga_2O_3

68.2 g of gallium nitrate hydrate (as supplied, Aldrich Chemical Co.) was dissolved in 150 ml of distilled water. Ammonia solution (35%) was added whilst stirring, until the solution gelled. The resultant solid was filtered and dried for 3 days at 60 °C. The solid was then heated at 500 °C for 12 h to produce α-Ga_2O_3.

δ-Ga_2O_3 was prepared by heating 27.3 g of gallium nitrate hydrate for 18 h at 225 °C. The ε-Ga_2O_3 was formed by taking this sample and subsequently grinding it in a pestle and mortar followed by further heating for 10 h at 550 °C.

2.1.2 Ball-Milled Ga_2O_3

8 g of commercial β-gallium oxide (Aldrich Chemical Co.) was heated at 1000 °C for 10 h and then milled in an alumina vial, using two alumina balls (ball-to-powder ratio equals to 0.18), using a SPEX 8000M Mixer/Mill, for various lengths of time. After each time period a portion of the sample was removed for analysis. Subsequent ^{27}Al MAS NMR showed that low levels of corundum contamination occurred from the milling media, but this amounted to less than 1 wt% Al_2O_3, an order of magnitude smaller than when it was intentionally added to the sample.

2.1.3 Al_2O_3-Pinned Ga_2O_3

61.4 g of gallium nitrate hydrate was dissolved in 150 ml of water. Ammonia solution was added until the sample gelled. The resultant solid was filtered and dried at 60 °C overnight, ground using a pestle and mortar and mixed with 50 ml of butan-2-ol to form a slurry. 12.5 ml of aluminium tri-*sec*-butoxide (Aldrich Chemical Co.) was then added and the slurry stirred for 1 h. Water was then added until the slurry gelled. The solid was filtered, washed with water and dried at 80 °C over a weekend. The dried solid was ground using a pestle and mortar and heated for 12 h at 500 °C. This process resulted in a sample that was 10% alumina by weight, an amount shown to be optimum for Zener pinning by previous work [21].

2.1.4 SiO_2-Pinned Ga_2O_3

58 g of gallium nitrate hydrate was dissolved in 150 ml of water. To this a separate solution of 14 ml of tetraethylorthosilicate (TEOS) (Aldrich Chemical Co.) in 50 ml of ethanol was added and stirred for 1 h. Ammonia solution was added whilst stirring, until the solution gelled. The resultant solid was filtered and dried overnight at 60 °C. The solid was then ground in a pestle and mortar and heated at 500 °C for 12 h. This process resulted in a sample that was 15% silica by weight, which again was an amount chosen in light of previous work [21].

Portions of each sample (excluding the ball-milled samples) were subsequently annealed for 1 h in air at 600, 800, 1000 and 1200 °C.

2.2 NMR

^{71}Ga MAS NMR spectra were obtained at 14.1 T (producing a ^{71}Ga Larmor frequency of 183 MHz) using a probe with a diameter of 3.2 mm and a MAS rate of 15–20 kHz. All shifts reported are referenced to $Ga(H_2O)_6^{3+}$ at 0 parts per million (ppm), for which a 3 μs pulse produced a 90° tip angle. For the powder

Ga_2O_3 samples, a spin-echo sequence ($1-\tau-2$ μs) was used with a recycle delay of 10 s and the time set to the reciprocal of the MAS frequency. Each spectrum took between 4 and 24 h to obtain (the longer times being required to obtain acceptable signal-to-noise ratios for the more disordered samples).

^{27}Al MAS NMR experiments were conducted in a 14.1 T magnetic field (^{27}Al Larmor frequency of 156.4 MHz) with a probe with a diameter of 3.2 mm spinning samples at about 20 kHz. These spectra were referenced against yttrium aluminium garnet (YAG), with the signal corresponding to the octahedrally coordinated aluminium site set to 0.7 ppm so that chemical shifts reported are relative to the primary shift reference of 1 M $[Al(H_2O)_6]^{3+}$ at 0 ppm. A pulse width of 9 μs produced a tip angle of 90° in the liquid $[Al(H_2O)_6]^{3+}$ sample. For the solid samples, a one-pulse sequence was used with a 0.5 μs pulse and a preacquisition delay of 7.5 μs and a recycle delay of 1 s, with an overall acquisition time of between 5 and 15 min for each sample. By varying the recycle delay between 1 and 10 s, no change was detected in the ratio of the different aluminium species detected. Certain ^{27}Al MAS NMR spectra were also recorded with similar parameters at 18.8 T using a probe with a diameter of 2.5 mm.

^{29}Si MAS NMR spectra were obtained using a 7.05 T magnet (giving a ^{29}Si Larmor frequency of 59.6 MHz) with a MAS probe with a diameter of 7 mm spinning the samples at 4 kHz. These were referenced using the signal from tetramethylsilane set to 0 ppm. A one-pulse sequence was used with a pulse width of 1.5 μs, which produced a tip angle of about 30°. The recycle delay was set to 20 s (sufficient to allow full relaxation), with a preacquisition delay of 30 μs. The average acquisition time for each sample was generally longer than for the other nuclei at 24–48 h due to the relatively low natural abundance of the ^{29}Si isotope (4.7%) and the small amount of silica in the samples (15% by weight).

All MAS NMR spectra were recorded using the Spinsight program and Varian Chemagnetics CMX, Infinity or Infinity Plus spectrometers. The dmfit2003 program [22] and QuadFit [23] were used to simulate the spectra and fit the peaks.

2.3 X-ray Diffraction

X-ray diffraction (XRD) experiments were conducted on a Philips PW 1720 diffractometer with Cu Kα radiation (0.1541 nm) and the resultant data were analyzed by the Traces v3.0 (Diffraction Technology, Pty) software, which also estimated the average metal oxide nanocrystal sizes via the Scherrer relation.

2.4 Electron Microscopy

Electron micrographs were obtained using a Zeiss SUPRA 55VP scanning electron microscope (SEM) with a 10 keV electron beam, and a Jeol 2000FX transmission electron microscope (TEM) with a 200 keV beam. Samples were prepared for the TEM by sonic dispersion in acetone and subsequent deposition on a holey carbon grid.

3 Results and Discussion

3.1 Sol-Gel Ga_2O_3

Figure 1 shows the ^{71}Ga MAS NMR spectrum obtained from the pure nanocrystalline Ga_2O_3 sample manufactured by the sol-gel method from gallium nitrate hydrate. A phase change from α to β occurred in the sample between 600 and 800 °C, as shown by ^{71}Ga MAS NMR and XRD (Fig. 2), accompanied by a reduction in average nanocrystal size. By 1200 °C, the crystallites had grown significantly to 272 nm in diameter, which is too large to be strictly termed nanocrystalline. The spectra for these phases seem highly complex at first, but most of the features present are actually spinning sidebands arising from the second-order quadrupolar broadened central transition, whose shapes are complex due to the nature of the interactions. While these can pose a significant problem in fitting the spectra, they can be identified as features which alter position as the MAS rate is varied. Figure 3a shows the ^{71}Ga MAS NMR spectrum for pure α-Ga_2O_3, which has one octahedrally coordinated gallium site. As shown in Table 1, this peak occurred at an isotropic chemical shift of 52 ppm with a χ_Q of 8.16 MHz and an asymmetry parameter of zero (i.e., an axially symmetric octahedral site). Figure 3b shows the spectrum obtained from pure β-Ga_2O_3. The feature labelled with an arrow was observed to remain static, along with the main second-order quadrupole line shape, as the spinning rate was al-

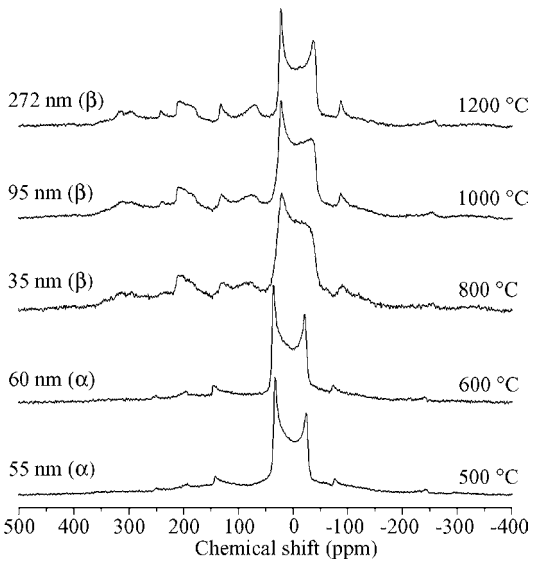

Fig. 1. ^{71}Ga MAS NMR spectra of pure nanocrystalline Ga_2O_3 produced by the sol-gel method, recorded at 14.1 T. Sizes given on the left are the average crystallite sizes as measured by XRD, with the phases given in brackets. Temperatures on the right are the temperatures at which each sample was annealed.

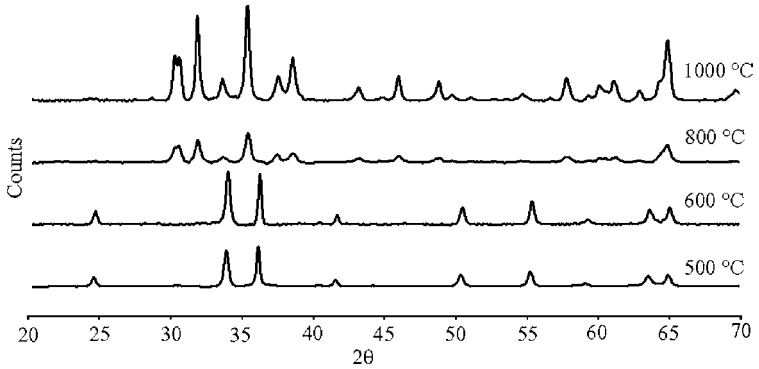

Fig. 2. XRD spectra obtained from the unpinned sol-gel Ga_2O_3 samples. The 500 and 600 °C spectra show the characteristic spectrum of the α-Ga_2O_3 phase, and the 800 and 1000 °C spectra show the β-Ga_2O_3 phase. For each of these two phases, the Bragg peaks narrow with increasing annealing temperature as the Ga_2O_3 crystals grow.

tered, and can therefore be identified as belonging to the tetrahedrally coordinated gallium site present in the β-phase. Multifield and single-crystal static NMR studies [3, 14, 15, 24] have reported parameters for the two gallium sites in β-Ga_2O_3, and these are also given in Table 1. In particular, the single-crystal work on twinned crystals produced highly accurate values for both the ^{71}Ga and ^{69}Ga NMR parameters, as well as the anisotropies and asymmetries of the chemical shift tensors [14]. The spectra were modelled using these values, and a good fit was obtained with minor modifications to the chemical shifts (see Table 1 and Fig. 3c). Note that in Fig. 3c the simulations of the two lines are not of the correct inten-

Table 1. Parameters obtained for the ^{71}Ga MAS NMR spectra of the α- and β-phases of Ga_2O_3, along with values reported in the literature.[a]

Ga_2O_3 phase	Ga coordination	δ (ppm)	χ_Q (MHz)	η
Alpha	Octahedral	52 (1)	8.16 (0.01)	0.00 (0.05)
Beta	Tetrahedral	201 (2)	11.1[b]	0.85[b]
	Octahedral	41 (1)	8.34[b]	0.1[b]
Beta (Massiot et al. [24])	Tetrahedral	200[c]	11[c]	0.85[c]
	Octahedral	40[c]	8.3[c]	0.08[c]
Beta (Vosegaard et al. [3], [14])	Tetrahedral	196.4 (1.6)	11.20 (0.03)	0.844 (0.007)
	Octahedral	25 (1)	8.34 (0.03)	0.094 (0.008)
Alpha (Ash and Grandinetti [15])	Octahedral	56 (7)	8.2 (0.1)	0.08 (0.04)
Beta (Ash and Grandinetti [15])	Tetrahedral	200 (50)	11.0 (0.5)	0.90 (0.1)
	Octahedral	50 (10)	8.2 (0.1)	0.12 (0.08)

[a] In parentheses, values for uncertainties are given.
[b] Values for the quadrupole parameters are based on the values of the single-crystal work in ref. 3 and are not fitted.
[c] No errors quoted.

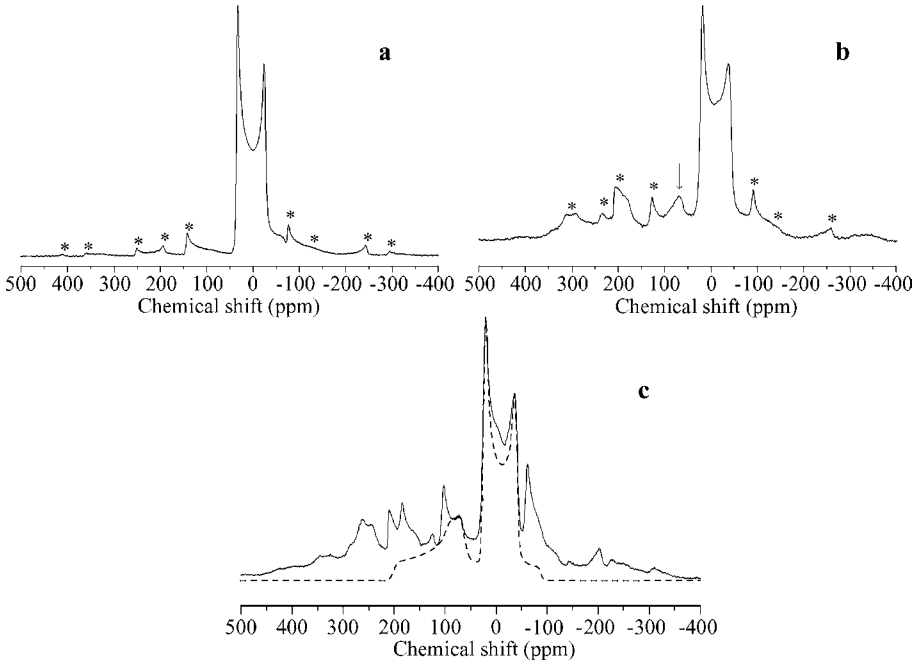

Fig. 3. ^{71}Ga MAS NMR spectra of α-Ga_2O_3 at 20 kHz MAS (**a**), β-Ga_2O_3 at 20 kHz MAS (**b**) and β-Ga_2O_3 at 15 kHz MAS (with the dashed line for simulation of the spectrum) (**c**), at 14.1 T. The asterisks denote spinning sidebands, and the arrow shows part of the Ga^{IV} line shape.

sity, this figure is merely an illustration of their line shapes and positions in relation to the experimental spectrum. The same values were used to run a time-domain simulation of the spectra by the SIMPSON program [25]. Figure 4 shows the results of this simulation, with the spectrum for each gallium site also shown separately. The simulated spectrum for the Ga^{IV} site shows a significantly lower intensity than that for the Ga^{VI} site. This is as expected since the much larger quadrupole interaction at the tetrahedrally coordinated site means under the conditions used (MAS and radio frequency) only partial excitation of the sites occurs.

The top three spectra in Fig. 1 show a quadrupolar line shape corresponding to the octahedrally coordinated gallium environment in β-Ga_2O_3 that becomes more well defined as the annealing temperature increases (illustrated by the sharpening of the two singularities). This demonstrates an increasingly ordered structure. Simulation of the line shape was carried out with QuadFit [23], using a Gaussian distribution in χ_Q values centered at 8.34 MHz (the value obtained from a bulk crystalline sample). The width of this distribution could then be used as a quantifiable reflection of the amount of disorder in the sample. Here, the assumption is being made that there is no interdependence between the various NMR parameters (e.g., for these simulations the asymmetry parameter was kept at zero at all times). Examples of such simulations are given in Fig. 5, and results are pre-

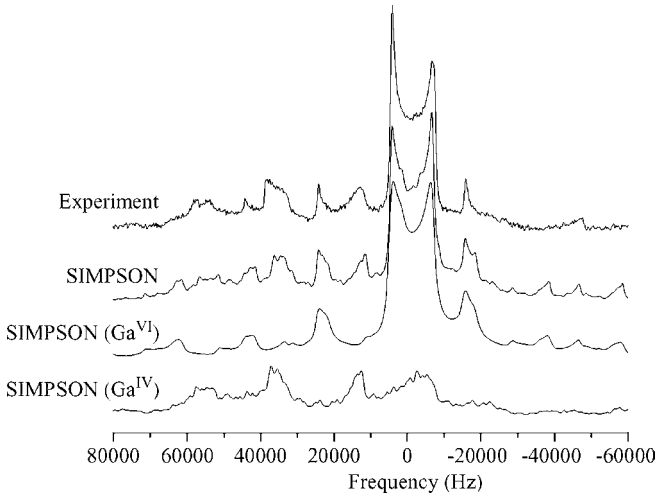

Fig. 4. SIMPSON simulations of the ^{71}Ga MAS NMR spectrum of β-Ga_2O_3 at 14.1 T, with a MAS rate of 20 kHz.

sented in Table 2. Uncertainties shown in Table 2 were estimated by varying $\Delta\chi_Q$ and visually checking the accuracy of the fit. Now several different approaches could be taken here, for example, static work would not be complicated by the fact that only a subset of sites (i.e., those with the smaller χ_Q values [12]) may be narrowed if the MAS is not fast enough. The complication with static spectra is that in the absence of MAS other interactions remain (e.g., dipolar coupling, chemical shift anisotropy) in addition to the distributions. The determination of distributions by this MAS NMR approach has been applied to ^{23}Na in glasses [26]. A similar approach is being applied here and it should give a semiquantitative measure of the changes in the order as the experimental conditions are being kept constant and the mean χ_Q is not changing within the error.

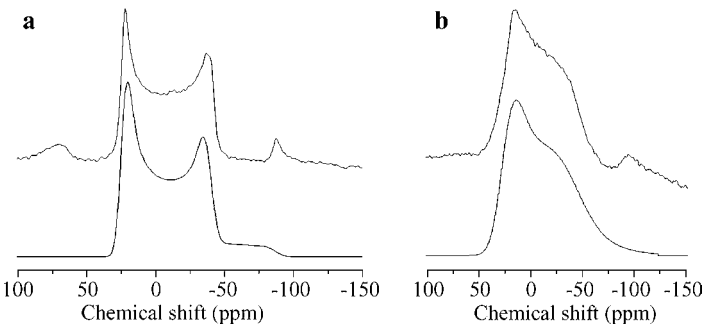

Fig. 5. Examples of simulations of the Ga^{VI} line of the β-Ga_2O_3 samples for the unpinned sol-gel sample annealed at 1200 °C (**a**) and the ball-milled sample milled for 1800 min (**b**). The top line is the experimental spectrum and the bottom line is the simulation.

Table 2. χ_Q distribution widths for the octahedral ^{71}Ga MAS NMR line of various samples. χ_Q distributions are centered at 8.34 MHz.*

β-Ga_2O_3 sample	Annealing temperature (°C)	Milling time (min)	χ_Q distribution width (MHz)
Pure sol-gel	800		1.75 (0.10)
	1000		1.55 (0.10)
	1200		0.40 (0.05)
Al_2O_3-pinned	800		1.90 (0.15)
	1000		1.70 (0.15)
	1200		1.20 (0.10)
SiO_2-pinned	1200		0.35 (0.05)
Ball-milled		0	0.60 (0.05)
		60	0.85 (0.05)
		600	1.80 (0.10)
		1800	2.20 (0.15)

* In parentheses, values for uncertainties are given.

3.2 Ball-Milled Ga_2O_3

Figure 6 shows the ^{71}Ga MAS NMR spectra of the ball-milled β-Ga_2O_3 samples. In this case, the distribution width of χ_Q values increases with milling time (Table 2), resulting in a significant broadening of the quadrupolar line shape after milling for 1800 min. This indicates the appearance of a significant amorphous region, which becomes a larger fraction of the sample with increasing milling time. The

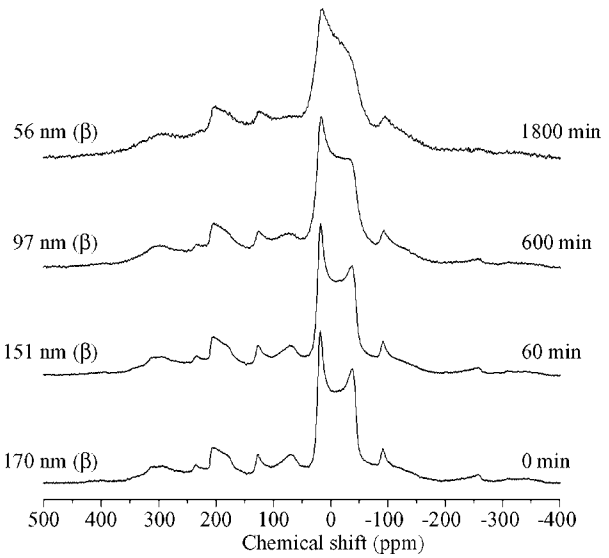

Fig. 6. ^{71}Ga MAS NMR spectra of the ball-milled samples at 14.1 T, each milled for the amount of time shown on the right.

nature of the mechanical attrition process means that energy is put into the oxide to cause such structural disorder. These ball-milled samples have undergone no annealing, which would likely remove such amorphous regions but would also promote growth of the crystallites.

3.3 Alumina-Pinned Ga_2O_3

Figure 7 shows the ^{71}Ga MAS NMR spectra for alumina-pinned Ga_2O_3 samples. The structural evolution of this system is very similar to the pure sol-gel manufactured Ga_2O_3 shown in Fig. 1. The Ga_2O_3 nanocrystals undergo the α-to-β phase transition between 600 and 800 °C, accompanied by a reduction in crystallite size. In this system, however, the presence of the alumina pinning phase has resulted in smaller crystallite sizes at higher temperatures (e.g., 117 nm after annealing at 1200 °C, compared with 272 nm in the unpinned sample as determined by XRD). As before, the octahedral line shapes of the β-phase spectra can be fitted with χ_Q distributions, and the results of this are given in Table 2.

Figure 8a shows the ^{27}Al MAS NMR spectra obtained from the alumina pinning phase in this system. Two main peaks are visible across the range of temperatures at around 15 and 65 ppm, and analogously to the ^{71}Ga spectra, these represent octahedrally and tetrahedrally coordinated aluminium sites, respectively [3, 27]. There is also a low-intensity, broad peak in between these features at the lower temperatures, representing five-coordinated aluminium and indicating

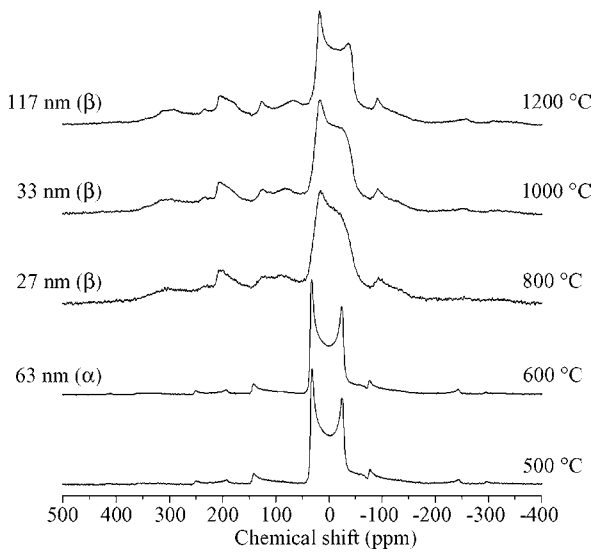

Fig. 7. ^{71}Ga MAS NMR spectra of the alumina-pinned Ga_2O_3 samples at 14.1 T. For the 500 °C sample, the XRD spectrum was unable to provide an estimate of the nanocrystal sizes due to the peaks being too broad to reliably fit.

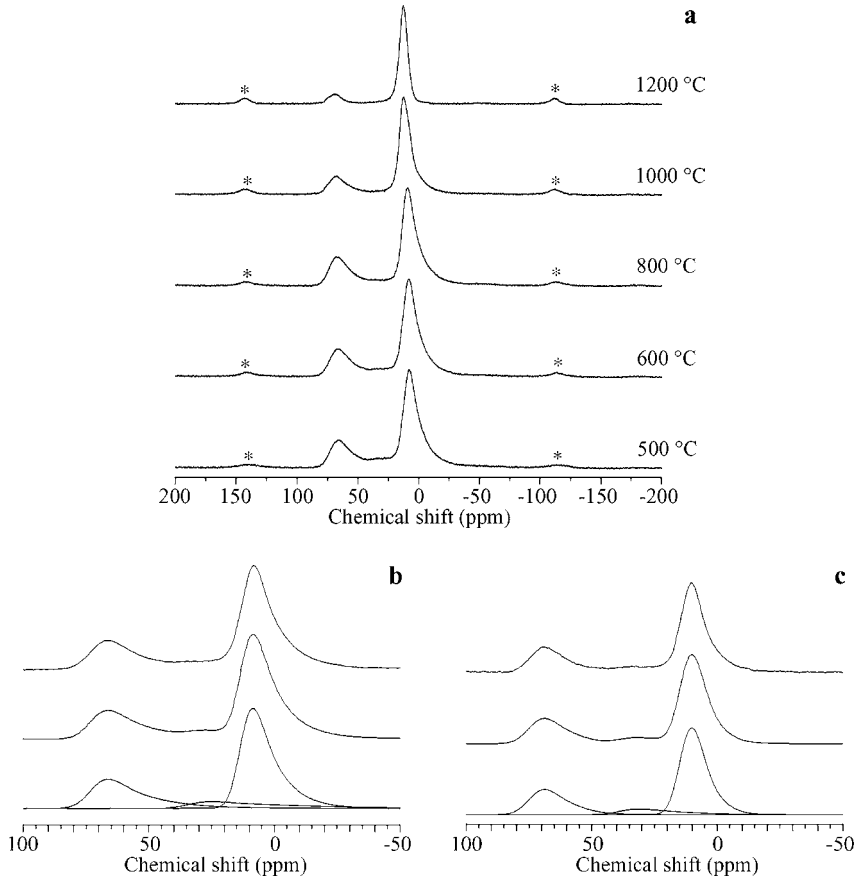

Fig. 8. **a** ^{27}Al MAS NMR spectra obtained from the alumina-pinned Ga_2O_3 samples. Spinning sidebands are labelled with asterisks. **b** and **c** Simulations of the sample annealed at 600 °C at 14.1 T (**b**) and 18.8 T (**c**). The top line is the experimental data, the bottom shows the individual simulated peaks, and the middle line is the net simulated spectrum.

Table 3. χ_Q distributions for the ^{27}Al MAS NMR spectra of the alumina-pinned Ga_2O_3 samples annealed at 600 and 1200 °C, obtained from two-field simulations.

Annealing temperature (°C)	Aluminium coordination	δ_{ISO} (ppm)	Mean χ_Q (MHz)[a]	χ_Q distribution width (MHz)[a]	Relative intensity (%)
600	4	75 (1)	8	6	27 (1)
	5	42[b] (4)	12[b]	6[b]	10[b] (2)
	6	14 (1)	6	5	63 (2)
1200	4	75 (1)	5	4	15 (2)
	6	13 (2)	0.5	0.5	85 (2)

[a] Error is ±0.5 MHz.

[b] Uncertainties for these values are large due to the broad and shallow nature of the line shape.

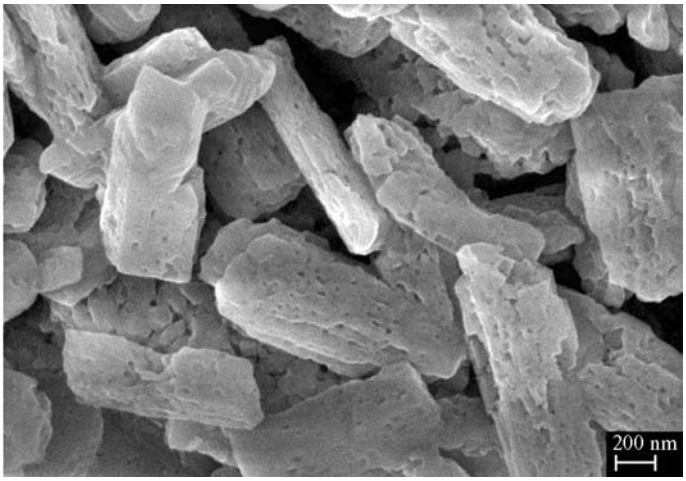

Fig. 9. SEM micrograph of the alumina-pinned Ga_2O_3 crystallites after annealing at 1200 °C.

disorder, which is (like the ^{71}Ga spectra) also conspicuous as a large distribution in χ_Q values (relative to the mean χ_Q), which causes the asymmetric line shape. Figure 8b and c shows two-field simulations of the 600 °C sample, allowing these χ_Q distributions (given in Table 3) to be more accurately constrained. 10% of the aluminium in the 600 °C sample exists in a five-coordinated site, and this decreases with annealing to zero at 1200 °C, where the octahedral aluminium line is almost symmetric and has a χ_Q distribution width of just 0.5 MHz. The alumina is crystalline at higher temperatures (as shown by XRD and SEM), with relatively little disorder, and is most likely to be the θ-Al_2O_3 transition alumina phase (with the confinement between the Ga_2O_3 crystallites preventing the transformation to the stable corundum form).

Figure 9 shows an SEM image of the alumina-pinned Ga_2O_3 system after annealing at 1200 °C. The Ga_2O_3 crystallites present are rectangular in shape, measuring approximately 200 by 400 by 1000 nm. Nanocrystalline Ga_2O_3 is well known to exhibit preferential growth in certain directions, frequently forming nano-ribbons and belt structures [28–30], and these favored growth directions can explain the shape of these crystals.

3.4 Silica-Pinned Ga_2O_3

Figure 10 shows the ^{71}Ga MAS NMR spectra obtained from the silica-pinned Ga_2O_3 samples. Immediately apparent is the highly significant degree of disorder present in the samples annealed at 500, 600 and 800 °C, resulting in broad and largely featureless NMR spectra. XRD results for these particular samples showed no Bragg reflections at all, indicating that they are either amorphous or

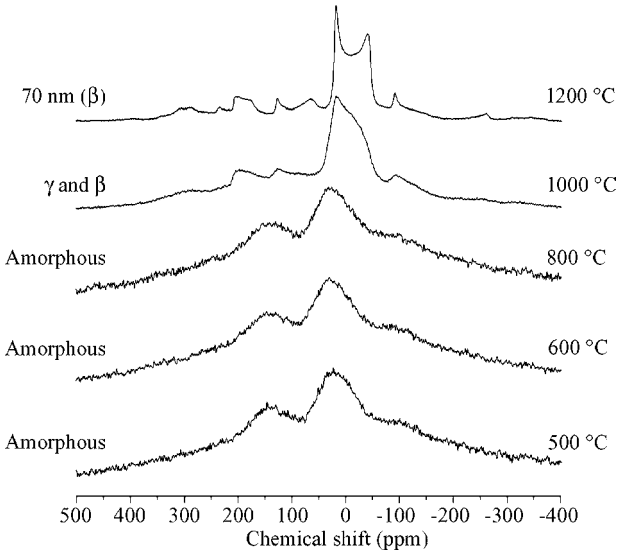

Fig. 10. ^{71}Ga MAS NMR spectra obtained from the silica-pinned Ga_2O_3 samples at 14.1 T.

consist of Ga_2O_3 and SiO_2 particles that are simply too small to be observed by XRD. This is why Zener pinning particles in nanocrystalline systems are generally difficult to observe by XRD, since they are expected to be at least an order of magnitude smaller than the nanocrystals they are pinning.

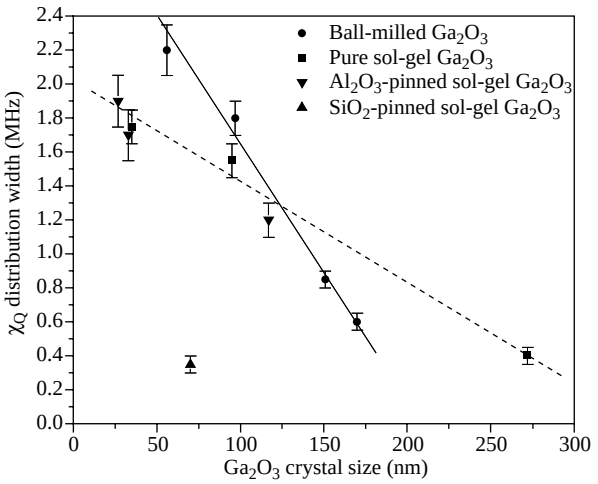

Fig. 11. χ_Q distribution widths for the octahedral ^{71}Ga MAS NMR line of β-phase samples manufactured by sol-gel or ball-milling versus average crystallite size. Solid line denotes to the linear fit of ball-milled Ga_2O_3 and dashed line denotes to the linear fit of pure sol-gel Ga_2O_3.

At 1000 °C the samples show two crystalline Ga_2O_3 phases in the XRD pattern (β and γ), and by 1200 °C only the β-phase remains, with a much smaller Ga_2O_3 nanocrystal size (70 nm, determined by XRD) compared with the pure sol-gel (272 nm) or alumina-pinned samples (117 nm) after annealing at the same temperature. The line shape of the octahedral gallium site in this spectrum is well defined, with a distribution in χ_Q of just 0.35 ± 0.05 MHz.

Figure 11 shows the χ_Q distribution widths against Ga_2O_3 crystallite sizes for all the samples described so far (from Table 2). It can be seen that for the ball-milled samples in the nanocrystalline region (<100 nm) there is significantly more inherent disorder than for the sol-gel prepared samples, indicated by higher χ_Q distribution widths. This is in agreement with previous reports of ball-milled nanocrystalline samples, in which a significant amorphous fraction was formed at the grain boundaries [31, 32]. The pure and alumina-pinned sol-gel prepared samples seem to lie on the same line, indicating that the alumina phase has little effect on the amount of disorder present in the Ga_2O_3. The silica-pinned sample, on the other hand, shows a much narrower χ_Q distribution than all the other samples of comparable nanocrystal diameters, meaning that the Ga_2O_3 nanocrystals are more highly crystalline and suggesting that the silica phase has the effect of reducing the inherent disorder of the Ga_2O_3 nanocrystals as well as restricting

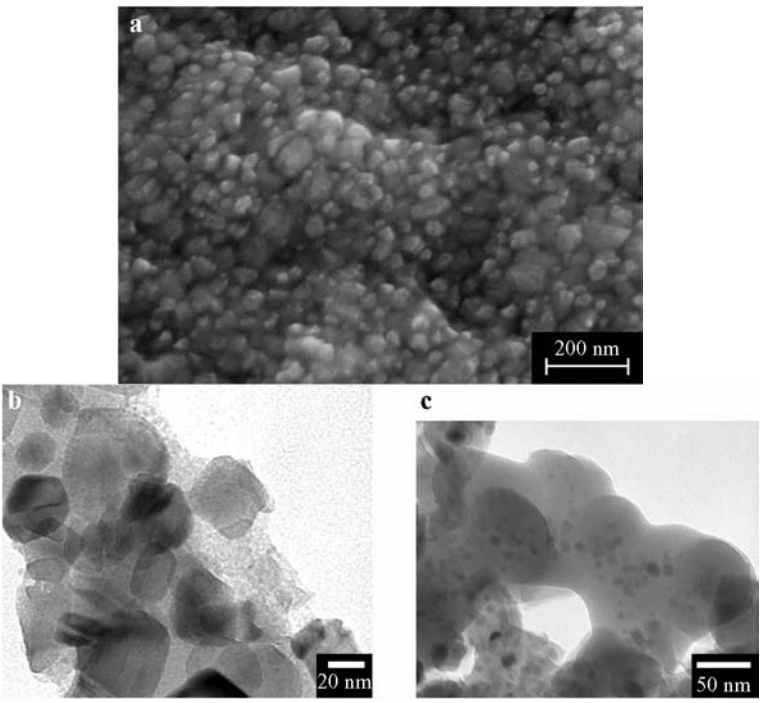

Fig. 12. a SEM image of the silica-pinned nanocrystalline Ga_2O_3 after annealing at 1200 °C. **b** and **c** TEM images of the silica-pinned Ga_2O_3 samples after annealing at 1200 °C.

their growth. These distributions in χ_Q likely represent distributions in both the bond lengths and bond angles around the Ga^{VI} site, although the contribution that each of these effects has on $\Delta\chi_Q$ is not distinguished here.

The SEM image in Fig. 12a shows that the silica-pinned Ga_2O_3 nanocrystals are well-aggregated with very little intercrystal porosity. The nanocrystal diameters in the image range from 20 to 80 nm. Closer inspection of this sample by TEM reveals two morphologies of the silica phase, a coating-like structure visible in Fig. 12b and discrete particles visible as dark spots in Fig. 12c. This range of morphologies is reflected in the ^{29}Si MAS NMR results (Fig. 13) as a distribution in Q^n species across the entire range of annealing temperatures (Table 4). Even in the sample annealed at 1200 °C, the full range of Q^n species is present ($0 \leq n \leq 4$), which is rare in a sol-gel produced silica annealed at such a high temperature (in a previous study [19], a pure sol-gel silica prepared from

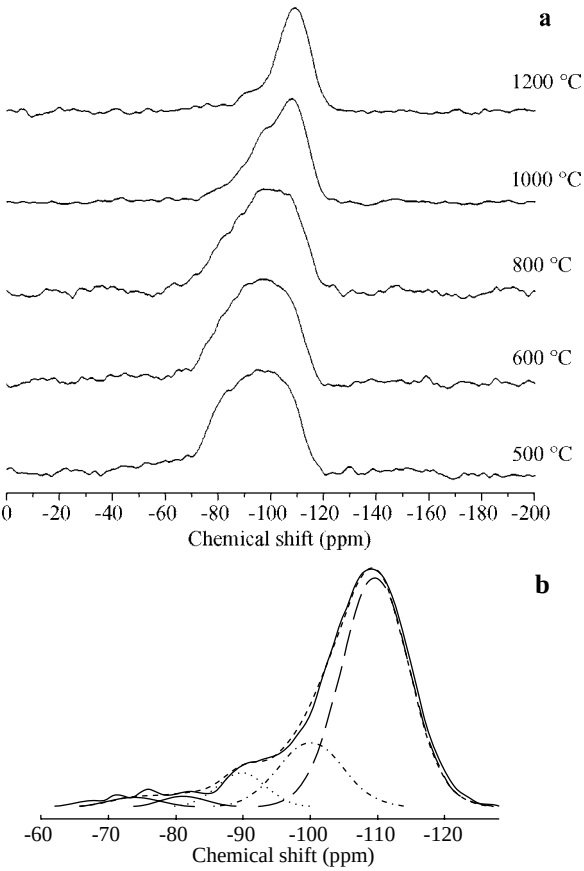

Fig. 13. a ^{29}Si MAS NMR spectra obtained from the silica-pinned Ga_2O_3 samples heated at various temperatures (7.05 T), **b** ^{29}Si MAS NMR simulation of the 1200 °C spectrum, showing the individual Q^n species as separate Gaussian peaks.

Table 4. ^{29}Si MAS NMR simulation data for the silica-pinned Ga_2O_3 samples.

Annealing temperature (°C)	δ (ppm)[a]	Peak width (Hz)[b]	Relative intensity (%)[c]	Q^n species
500	−110	670	9	4
	−101	1100	41	3
	−89	1060	30	2
	−81	750	13	1
	−64	1410	8	0
600	−109	560	10	4
	−101	950	42	3
	−90	850	27	2
	−80	920	18	1
	−69	710	3	0
800	−110	620	19	4
	−100	870	39	3
	−90	860	25	2
	−80	900	14	1
	−71	600	2	0
1000	−110	690	46	4
	−100	780	34	3
	−91	660	14	2
	−80	660	6	1
1200	−110	710	70	4
	−100	670	19	3
	−90	500	7	2
	−81	450	2	1
	−74	500	2	0

[a] Error is ±2 ppm.
[b] Error is ±30 Hz.
[c] Error is ±2%.

TEOS showed only Q^4 species present after annealing at 1000 °C, i.e., the silica network was fully connected). Some of the silica pinning particles visible in Fig. 12c are below 5 nm in diameter, and so the amount of surface silicon sites, which likely exist as Q^3 or Q^2, will be relatively high. The presence of small amounts of Q^1 and Q^0 species (around 4%) at such a high temperature is difficult to explain because hydroxyl groups should be completely removed by 800 °C. Although the ^{29}Si NMR data was simulated by keeping the chemical shifts of the five Q^n species as close as possible to their standard values [12] for consistency with other results (whilst retaining an accurate fit of the line shape), it is possible that these lower-order sites are actually highly distorted Q^2 species in a disordered silica phase (e.g., the coating in Fig. 12b).

It should be noted that although the full range of Q^n species appears to remain present as the annealing temperature is increased, the general trend is towards higher n values (e.g., 9% of the silicon exists in a Q^4 site at 500 °C compared with 70% at 1200 °C). The decrease in the spread of Q^n species is quali-

tatively apparent in Fig. 13 as a narrowing of the overall spectral line and a shift to the right. This trend is regularly observed in materials of this type, as hydroxyl groups are removed and the network becomes more interconnected [33–35].

3.5 δ-Ga_2O_3

Figure 14a shows the ^{71}Ga MAS NMR spectrum of about 11 nm dimensioned δ-Ga_2O_3, and the simulation of this spectrum. Immediately apparent is the fact that this sample contained an extremely large amount of disorder, present as an extremely broad underlying peak across the range from 650 to −700 ppm. This feature was simulated as a standard Gaussian peak. This amorphous fraction arises due to both the extremely small sizes of the Ga_2O_3 nanocrystals (11 nm) and also the much lower annealing temperature compared with the other samples discussed above (225 °C), which means that a significant amount of hydroxyl groups remain present in the sample (i.e., it has not fully crystallized). Nonetheless, XRD

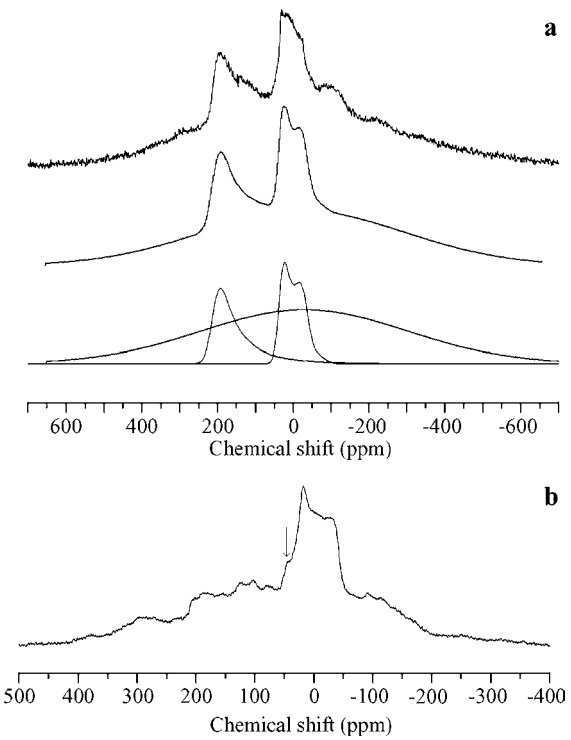

Fig. 14. a ^{71}Ga MAS NMR spectrum obtained from δ-Ga_2O_3 (top line), the simulated spectrum (middle line) and the individual simulated peaks (bottom lines). **b** ^{71}Ga MAS NMR spectrum of a mixture of β- and ε-Ga_2O_3 nanocrystalline phases. The shoulder indicated with an arrow may be due to the octahedral gallium site in ε-Ga_2O_3. Both spectra were recorded at 14.1 T.

Table 5. Simulation data for the δ-Ga_2O_3 sample. The broad amorphous region comprised 71% of the spectral intensity, with the remainder split equally between the tetrahedral and octahedral gallium peaks. Uncertainties here are relatively large due to the broad nature of the spectral lines.

Ga coordination	δ_{ISO} (ppm)	χ_Q (MHz)	χ_Q distribution width (MHz)	η	Intensity (%)
Octahedral	52 (4)	8.5 (1)	1	0	15 (3)
Tetrahedral	210 (4)	7 (1)	12	0	14 (3)
Amorphous region	–	–	–	–	71 (5)

results show that crystalline δ-Ga_2O_3 is present, and so an attempt to simulate the NMR spectrum was made and these results are given in Table 5. Disorder is also indicated here by a significant distribution in χ_Q values.

The features in the spectrum not accounted for by the simulation (e.g., the broad feature at around −100 ppm) are assumed to be spinning sidebands. The inherent disorder in the sample and lack of any sharp spectral features makes the simulation somewhat ambiguous, and so these parameters are tentative. Since δ-Ga_2O_3 should exist as a C-type rare-earth oxide structure [6], which contains only octahedrally coordinated gallium sites [36], the tetrahedral line can be assumed to be a result of hydroxyl groups remaining attached to gallium atoms and preventing complete conversion to δ-Ga_2O_3. Hence only the parameters for the octahedral line may apply to the δ-Ga_2O_3 phase.

3.6 ε-Ga_2O_3

Figure 14b shows the ^{71}Ga MAS NMR spectrum of the same sample in Fig. 14a but this time annealed at 800 °C. The XRD results from this sample indicated the presence of both the β- and ε-phases, with the phase existing as about 27 nm nanocrystals. A significant amorphous component remains in this sample, although a Gaussian simulation of it showed that it had been reduced to just about 33% of the overall spectral intensity, indicating some further crystallization. This spectrum is impossible to fit reliably (even though the parameters for the β-phase are already known) due to so many broad overlapping peaks, and spinning sidebands for each of these. A shoulder on the left-hand side of the octahedral peak (labelled with an arrow in Fig. 13b) could possibly be due to the octahedral gallium site in ε-Ga_2O_3, but this is only a small feature in a very complicated spectrum. In order to obtain a less ambiguous set of results, either a pure ε-Ga_2O_3 sample must be studied or different experimental techniques must be used.

4 Conclusions

^{71}Ga MAS NMR parameters are reported for three phases of nanocrystalline Ga_2O_3, with a relatively high accuracy for the α- and β-phases, but with a much larger uncertainty in the case of δ.

Silica-pinning particles have been shown to have a much stronger pinning effect than alumina, with the silica-pinned Ga_2O_3 nanocrystals containing much less inherent disorder than the alumina-pinned, pure sol-gel and ball-milled samples. Silica-pinned nanocrystalline Ga_2O_3 showed crystal sizes of just 70 nm after annealing at 1200 °C, compared with 272 nm for the unpinned sample. The silica phase exists in a range of morphologies, with a high degree of disorder present even at higher annealing temperatures, as demonstrated by the range of Q^n species that persist up to 1200 °C. The alumina-pinning phase exists as crystalline θ-Al_2O_3 at the high annealing temperatures. Ball-milling is shown quantitatively by NMR to produce nanocrystalline samples with a much higher degree of disorder than sol-gel produced samples of similar crystallite sizes. This is attributed to the mechanical attrition nature of the formation process which introduces energy to the system, and also the fact that the ball-milled samples are not annealed. It is clear that the silica and alumina show varying degrees of success at pinning; however, the silica-pinning phase seemed to also have an effect on the inherent disorder within the β-Ga_2O_3 crystals, showing a much narrower $\Delta\chi_Q$ for the Ga^{VI} site than the unpinned or alumina-pinned samples with comparable nanocrystal diameters. The reason for this effect is currently unclear.

Acknowledgments

The Engineering and Physical Sciences Research Council (EPSRC) is thanked for funding the collaboration between Warwick and Kent on nanocrystalline materials through grants (GR/S61881 and GR/S61898). M.E.S. thanks both EPSRC and the University of Warwick for partial funding of NMR equipment at Warwick. Steve York is also thanked for his help with the electron microscopy.

References

1. Machon, D., McMillan, P.F., Xu, B., Dong, J.: Phys. Rev. B **73**, 094125 (2006)
2. Roy, R., Hill, V.G., Osborn, E.F.: J. Am. Chem. Soc. **74**, 719–722 (1952)
3. Massiot, D., Vosegaard, T., Magneron, N., Trumeau, D., Montouillout, V., Berthet, P., Loiseau, T., Bujoli, B.: Solid State Nucl. Magn. Reson. **15**, 159–169 (1999)
4. Zinkevich, M., Aldinger, F.: J. Am. Ceram. Soc. **87**, 683–691 (2004)
5. Escribano, V.S., Amores, J.M.G., López, E.F., Panizzi, M., Resini, C., Busca, G.: J. Mater. Sci. **40**, 2013–2021 (2005)
6. Delgado, M.R., Areán, C.O.: Z. Anorg. Allg. Chem. **631**, 2115–2120 (2005)
7. Mathew, T., Yamada, Y., Ueda, A., Shioyama, H., Kobayashi, T.: Catal. Lett. **100**, 247–253 (2005)
8. Fleischer, M., Meixner, H.: Sens. Actuators B **4**, 437–441 (1990)
9. Li, Y., Trinchi, A., Wlodarski, W., Galatsis, K., Kalanter-zadeh, K.: Sens. Actuators B **93**, 431–434 (2003)
10. He, C., Paulus, M., Find, J., Nickl, J.A., Eberle, H.J., Spengler, J., Chu, W., Köhler, K.: J. Phys. Chem. B **109**, 15906–15914 (2005)
11. Smith, C.S.: Trans. Metall. Soc. **175**, 15–51 (1948)
12. MacKenzie, K.J.D., Smith, M.E.: Multinuclear Solid-State NMR of Inorganic Materials. Pergamon, London (2002)

13. Smith, M.E., van Eck, E.R.H.: Prog. Nucl. Magn. Reson. Spectrosc. **34**, 159–201 (1999)
14. Vosegaard, T., Byriel, I.P., Binet, L., Massiot, D., Jakobsen, H.J.: J. Am. Chem. Soc. **120**, 8184–8188 (1998)
15. Ash, J.T., Grandinetti, P.J.: Magn. Reson. Chem. **44**, 823–831 (2006)
16. Chadwick, A.V., Savin, S.L.P., O'Dell, L.A., Smith, M.E.: J. Phys. Condens. Matter **18**, L163–L170 (2006)
17. Savin, S.L.P., Chadwick, A.V., O'Dell, L.A., Smith, M.E.: Phys. Status Solidi **2**, 661–664 (2005)
18. Savin, S.L.P., Chadwick, A.V., O'Dell, L.A., Smith, M.E.: Solid State Ionics **117**, 2519–2526 (2006)
19. O'Dell, L.A., Savin, S.L.P., Chadwick, A.V., Smith, M.E.: Nanotechnology **16**, 1836–1843 (2005)
20. O'Dell, L.A., Savin, S.L.P., Chadwick, A.V., Smith, M.E.: Faraday Discuss. **134**, 83–102 (2007)
21. Al-Angari, Y., Ph.D. thesis, University of Kent, Canterbury, Kent, UK, 2002.
22. Massiot, D., Fayon, F., Capron, M., King, I., Le Calvé, S., Alonso, B., Durand, J.-O., Bujoli, B., Gan, Z., Hoatson, G.: Magn. Reson. Chem. **40**, 70–76 (2002)
23. Kemp, T.F., M. thesis, University of Warwick, Coventry, UK, 2004.
24. Massiot, D., Farnan, I., Gaultier, N., Trumeau, D., Trokiner, A., Coutures, J.P.: Solid State Nucl. Magn. Reson. **4**, 241–248 (1995)
25. Bak, M., Rasmussen, J.T., Nielsen, N.C.: J. Magn. Reson. **147**, 296–330 (2000)
26. Kohn, S.C., Smith, M.E., Dirken, P.J., van Eck, E.R.H., Kentgens, A.P.M., Dupree, R.: Geochim. Cosmochim. Acta **62**, 79–87 (1998)
27. Smith, M.E.: Appl. Magn. Reson. **4**, 1–64 (1993)
28. Gao, S., Xie, Y., Zhu, L., Tian, X.: Inorg. Chem. **42**, 5442–5447 (2003)
29. Zhang, J., Jiang, F., Yang, Y., Li, J.: J. Phys. Chem. B **109**, 13143–13147 (2005)
30. Gundiah, G., Govindaraj, A., Rao, C.N.R.: Chem. Phys. Lett. **351**, 189–194 (2002)
31. Chadwick, A.V., Pooley, M.J., Rammutla, K.E., Savin, S.L.P., Rougier, A.: J. Phys. Condens. Matter **15**, 431–440 (2003)
32. Heitjans, P., Masoud, M., Feldhoff, A., Wilkening, M.: Faraday Discuss. **134**, 67–82 (2007)
33. Pickup, D.M., Mountjoy, G., Wallidge, G.W., Newport, R.J., Smith, M.E.: Phys. Chem. Chem. Phys. **1**, 2527–2533 (1999)
34. Gunawidjaja, P.N., Holland, M.A., Mountjoy, G., Pickup, D.M., Newport, R.J., Smith, M.E.: Solid State Nucl. Magn. Reson. **23**, 88–106 (2003)
35. Wallidge, G.W., Anderson, R., Mountjoy, G., Pickup, D.M., Gunawidjaja, P., Newport, R.J., Smith, M.E.: J. Mater. Sci. **39**, 6743–6755 (2004)
36. Bloor, D., Dean, J.R.: J. Phys. C: Solid State Phys. **5**, 1237–1252 (1972)

Authors' address: Mark E. Smith, Department of Physics, University of Warwick, Coventry CV4 7AL, UK
E-mail: M.E.Smith.1@warwick.ac.uk